Inorg. Chem. **2008**, *47*, 6144−6152

Synthesis and Study of the Spectroscopic and Redox Properties of Ru^{II},Pt^{II} Mixed-Metal Complexes Bridged by 2,3,5,6-Tetrakis(2-pyridyl)pyrazine

Shengliang Zhao, Shamindri M. Arachchige, Carla Slebodnick, and Karen J. Brewer*

Department of Chemistry, Virginia Polytechnic Institute and State University, Blacksburg, Virginia 24061-0212

Received November 27, 2007

The mixed-metal supramolecular complexes $[(tpy)Ru(tppz)PtCl](PF_6)_3$ and $[ClPt(tppz)Ru(tppz)PtCl](PF_6)_4$ (tpy = 2,2′:6′,2″-terpyridine and tppz = 2,3,5,6-tetrakis(2-pyridyl)pyrazine) were synthesized and characterized. These complexes contain ruthenium bridged by tppz to platinum centers to form stereochemically defined linear assemblies. X-ray crystallographic determinations of the two complexes confirm the identity of the metal complexes and reveal intermolecular interactions of the Pt sites in the solid state for $[(tpy)Ru(tppz)PtCl](PF_6)_3$ with a Pt···Pt distance of 3.3218(5) Å. The ^1H NMR spectra show the expected splitting patterns characteristic of stereochemically defined mixed-metal systems and are assigned with the use of $^1H-^1H$ COSY and NOESY. Electronic absorption spectroscopy displays intense ligand-based $\pi \rightarrow \pi^*$ transitions in the UV and MLCT transitions in the visible. Electrochemically $[(tpy)Ru(tppz)PtCl](PF_6)_3$ and $[ClPt(tppz)Ru(tppz)PtCl](PF_6)_4$ display reversible $Ru^{II/III}$ couples at 1.63 and 1.83 V versus Ag/AgCl, respectively. The complexes display very low potential $tppz^{0/-}$ and $tppz^{-/2-}$ couples, relative to their monometallic synthons, $[(tpy)Ru(tppz)](PF_6)_2$ and $[Ru(tppz)_2](PF_6)_2$, consistent with the bridging coordination of the tppz ligand. The $Ru(d\pi) \rightarrow tppz(\pi^*)$ MLCT transitions are also red-shifted relative to the monometallic synthons occurring in the visible centered at 530 and 538 nm in CH_3CN for $[(tpy)Ru(tppz)PtCl](PF_6)_3$ and $[ClPt(tppz)Ru(tppz)PtCl](PF_6)_4$, respectively. The complex $[(tpy)Ru(tppz)PtCl](PF_6)_3$ displays a barely detectable emission from the $Ru(d\pi) \rightarrow tppz(\pi^*)$ ^{3}MLCT in CH_3CN solution at RT. In contrast, $[ClPt(tppz)Ru(tppz)PtCl](PF_6)_4$ displays an intense emission from the $Ru(d\pi) \rightarrow tppz(\pi^*)$ ^{3}MLCT state at RT with $\lambda_{max}^{em} = 754$ nm and $\tau = 80$ ns.

Introduction

The discovery of $[Ru(bpy)_3]^{2+}$ (bpy = 2,2′-bipyridine) and its desirable excited-state photochemical and photophysical properties has inspired much research toward exploiting this and related chromophores in solar energy conversion schemes.[1,2] Complicated multicomponent systems incorporating light absorber (LA) units, electron relays (ERs), and reactive metals (RMs) within the molecular architecture are desirable for efficient light to energy conversion processes. Within this perspective, polyazine bridging ligands (BLs) have been used to chemically bond the individual components into the same molecular framework, allowing the construction of complex polymetallic supramolecular species.[3] One of the most widely used polyazine bridging ligands is the bidentate ligand dpp (2,3-bis(2-pyridyl)pyrazine).[3−6] The dpp ligand acts as an AB chelate and binds two metal centers through a pyridyl and a pyrazine nitrogen. This mode of coordination of dpp affords polymetallic complexes that are stereochemically ill-defined, limiting the ability to control subunit orientation and distance within a supramolecular assembly, which is undesired for the rational design of assemblies capable of complex functions. The use of tridentate ligands in the construction of polymetallic systems

* To whom correspondence should be addressed. E-mail: kbrewer@vt.edu. Telephone: (540)-231-6579. Fax: (540)231-3255.

(1) Juris, A.; Balzani, V.; Barigelletti, F.; Campagna, S.; Belser, P.; Vonzelewsky, A. *Coord. Chem. Rev.* **1988**, *84*, 85–277.
(2) Kalyanasundaram, K. *Coord. Chem. Rev.* **1982**, *46*, 159–244.
(3) Balzani, V.; Juris, A.; Venturi, M.; Campagna, S.; Serroni, S. *Chem. Rev.* **1996**, *96*, 759–833.
(4) Campagna, S.; Di Pietro, C.; Loiseau, F.; Maubert, B.; McClenaghan, N.; Passalacqua, R.; Puntoriero, F.; Ricevuto, V.; Serroni, S. *Coord. Chem. Rev.* **2002**, *229*, 67–74.
(5) Fuchs, Y.; Lofters, S.; Dieter, T.; Shi, W.; Morgan, R.; Strekas, T. C.; Gafney, H. D.; Baker, A. D. *J. Am. Chem. Soc.* **1987**, *109*, 2691–2697.
(6) Braunstein, C. H.; Baker, A. D.; Strekas, T. C.; Gafney, H. D. *Inorg. Chem.* **1984**, *23*, 857–864.

10.1021/ic7023296 CCC: $40.75
Published on Web 06/24/2008

leads to stereochemically defined systems that have efficient control of subunit distance and orientation. The application of tridentate complexes in solar energy conversion schemes has been somewhat limited by the short metal-to-ligand charge-transfer (^{3}MLCT) excited-state lifetime of $[Ru(tpy)_2]^{2+}$ (tpy = 2,2′:6′,2″-terpyridine).[7,8] This short MLCT excited-state lifetime results from low-lying ligand field states that are thermally accessible at room temperature.

The design of tridentate complexes of Ru(II) with long-lived ^{3}MLCT excited states than $[Ru(tpy)_2]^{2+}$ is an ongoing area of research.[9–11] A recent review by Hanan highlights the variety of approaches being employed with much focus on tuning the energetics of the ^{3}LF and ^{3}MLCT states by component modification.[12] In line with this, long-lived excited-state lifetimes of the ^{3}MLCT states in Ru(II)-tpy-based systems have been achieved by substitution of electron-donating or -withdrawing substituents on the tpy ring system,[12] substitution of the nitrogen donor atoms on the pyridine rings with carbon leading to cyclometallated complexes that are stronger σ donors,[13,14] and construction of multimetallic complexes that possess bridging ligands with stabilized π*-acceptor orbitals. The excited-state lifetime of the ^{3}MLCT state has been extended successfully in these systems by limiting thermal population of the ^{3}LF state at room temperature, either through destabilization of the ^{3}LF state or stabilization of the ^{3}MLCT state.

Mixed-metal complexes containing the tridentate bridging ligand tppz (2,3,5,6-tetrakis(2-pyridyl)pyrazine) have been studied, providing stereochemically defined complexes, often with long-lived emissive ^{3}MLCT excited states.[15–18] Substitution of a tpy with tppz in $[Ru(tpy)_2]^{2+}$, lowers the energy of the ^{3}MLCT state as a result of the stabilized tppz(π*)-acceptor orbital. Coordination of a second Ru(II) center to the tppz affords a further stabilized ^{3}MLCT state with an even longer lived excited-state lifetime.[19] The complex $[(tpy)Ru(tppz)](PF_6)_2$ emits at 665 nm with a lifetime of 30 ns in RT CH_3CN solution, while the bridged system, $[(tpy)Ru(tppz)Ru(tppz)](PF_6)_4$, emits at 830 nm with a lifetime of 100 ns under the same conditions.[20] Recently, interesting reports of larger multimetallic systems of Ru(II) and tppz have appeared with theoretical studies proposing high degrees of delocalization of these complexes and the onset of band type electronic structure.[17,18] The study of mixed-metal systems with the tppz ligand are not widely reported with much work focused on Ru(II) and Os(II) systems.[19,20]

Some crystallographic studies of complexes of the tppz ligand are reported.[21–24] The tppz ligand is shown to coordinate to metals in a variety of unusual coordination environments, highlighted in a review by Pennington.[25] The tppz ligand binds in a tridentate fashion to two metal centers. In this coordination environment, distortion from planarity of the tppz ligand is necessary to relieve the steric interaction of the hydrogens on the 3-positions of the pyridine rings. X-ray crystallographic analysis of Ru(II),Pt(II) bridged systems are rare.[26,27]

The coupling of reactive metals to Ru(II) light absorbers is not well studied despite the promise such complexes hold in many forums including light-to-energy conversion schemes. We previously reported a mixed-metal Ru,Rh tppz complex, $[(tpy)Ru(tppz)RhCl_3](PF_6)_2$, that displayed quenching of the ^{3}MLCT state via electron transfer to generate a lower-lying Ru-to-Rh metal-to-metal charge transfer state.[28] The coupling of Ru(II) to Pt(II) within the stereochemically defined tridentate bridged architecture of tppz has not been reported. The use of bidentate ligands to bridge Ru(II) light absorbing units to reactive metals such as Pt(II) has been investigated.[29–34] The coupling of Pt(II) to Ru(II) in bidentate coordination environments to produce heterobimetallic complexes such as $[(bpy)_2Ru(dpp)PtCl_2]^{2+}$ lead to systems that possess further stabilized ^{3}MLCT excited states relative to the homo-bimetallic analogs, $[(bpy)_2Ru(dpp)Ru(bpy)_2]^{4+}$.

The study of square planar $[Pt(tpy)L]^{n+}$ (L = monodentate ligand) has been reported with focus being on interactions

(7) Kirchhoff, J. R.; McMillin, D. R.; Marnot, P. A.; Sauvage, J. P. *J. Am. Chem. Soc.* **1985**, *107*, 1138–1141.
(8) Young, R. C.; Nagle, J. K.; Meyer, T. J.; Whitten, D. G. *J. Am. Chem. Soc.* **1978**, *100*, 4773–4778.
(9) Fang, Y. Q.; Taylor, N. J.; Laverdiere, F.; Hanan, G. S.; Loiseau, F.; Nastasi, F.; Campagna, S.; Nierengarten, H.; Leize-Wagner, E.; Van Dorsselaer, A. *Inorg. Chem.* **2007**, *46*, 2854–2863.
(10) Abrahamsson, M.; Jager, M.; Osterman, T.; Eriksson, L.; Persson, P.; Becker, H. C.; Johansson, O.; Hammarstrom, L. *J. Am. Chem. Soc.* **2006**, *128*, 12616–12617.
(11) Abrahamsson, M.; Wolpher, H.; Johansson, O.; Larsson, J.; Kritikos, M.; Eriksson, L.; Norrby, P. O.; Bergquist, J.; Sun, L.; Akermark, B.; Hammarstrom, L. *Inorg. Chem.* **2005**, *44*, 3215–3225.
(12) Medlycott, E. A.; Hanan, G. S. *Coord. Chem. Rev.* **2006**, *250*, 1763–1782.
(13) Constable, E. C.; Hannon, M. J. *Inorg. Chim. Acta* **1993**, *211*, 101–110.
(14) Barigelletti, F.; Ventura, B.; Collin, J. P.; Kayhanian, R.; Gavina, P.; Sauvage, J. P. *Eur. J. Inorg. Chem.* **2000**, 113–119.
(15) Yuasa, J.; Fukuzumi, S. *J. Am. Chem. Soc.* **2006**, *128*, 15976–15977.
(16) Carlson, C. N.; Kuehl, C. J.; DaRe, R. E.; Veauthier, J. M.; Schelter, E. J.; Milligan, A. E.; Scott, B. L.; Bauer, E. D.; Thompson, J. D.; Morris, D. E.; John, K. D. *J. Am. Chem. Soc.* **2006**, *128*, 7230–7241.
(17) Fantacci, S.; DeAngelis, F.; Wang, J.; Bernhard, S.; Selloni, A. *J. Am. Chem. Soc.* **2004**, *126*, 9715–9723.
(18) Flores-Torres, S.; Hutchison, G. R.; Soltzberg, L. J.; Abruna, H. D. *J. Am. Chem. Soc.* **2006**, *128*, 1513–1522.
(19) Arana, C. R.; Abruna, H. D. *Inorg. Chem.* **1993**, *32*, 194–203.
(20) Vogler, L. M.; Brewer, K. J. *Inorg. Chem.* **1996**, *35*, 818–824.
(21) Campos-Fernandez, C. S.; Smucker, B. W.; Clerac, R.; Dunbar, K. R. *Isr. J. Chem.* **2001**, *41*, 207–218.
(22) Chanda, N.; Laye, R. H.; Chakraborty, S.; Paul, R. L.; Jeffrey, J. C.; Ward, M. D.; Lahiri, G. K. *J. Chem. Soc., Dalton Trans.* **2002**, 3496–3504.
(23) Padgett, C. W.; Walsh, R. D.; Drake, G. W.; Hanks, T. W.; Pennington, W. T. *Cryst. Growth Des.* **2005**, *5*, 745–753.
(24) Sakai, K.; Kurashima, M. *Acta Crystallogr. Sect. E: Struct. Rep. Online* **2003**, *59*, M411–M413.
(25) Padgett, C. W.; Pennington, W. T.; Hanks, T. W. *Cryst. Growth Des.* **2005**, *5*, 737–744.
(26) Yam, V. W.-W.; Lee, V. W.-M.; Cheung, K.-K. *J. Chem. Soc., Chem. Commun.* **1994**, 2075–2076.
(27) Van der Schilden, K.; Garcia, F.; Kooijman, H.; Spek, A. L.; Haasnoot, J. G.; Reedijk, J. *Angew. Chem., Int. Ed.* **2004**, *43*, 5668–5670.
(28) Lee, J. D.; Vrana, L. M.; Bullock, E. R.; Brewer, K. J. *Inorg. Chem.* **1998**, *37*, 3575–3580.
(29) Paw, W.; Connick, W. B.; Eisenberg, R. *Inorg. Chem.* **1998**, *37*, 3919–3926.
(30) Sommovigo, M.; Denti, G.; Serroni, S.; Campagna, S.; Mingazzini, C.; Mariotti, C.; Juris, A. *Inorg. Chem.* **2001**, *40*, 3318–3323.
(31) Miao, R.; Mongelli, M. T.; Zigler, D. F.; Winkel, B. S. J.; Brewer, K. J. *Inorg. Chem.* **2006**, *45*, 10413–10415.
(32) Williams, R. L.; Toft, H. N.; Winkel, B.; Brewer, K. J. *Inorg. Chem.* **2003**, *42*, 4394–4400.
(33) Swavey, S.; Fang, Z.; Brewer, K. J. *Inorg. Chem.* **2002**, *41*, 2598–2607.
(34) Ozawa, H.; Haga, M.; Sakai, K. *J. Am. Chem. Soc.* **2006**, *128*, 4926–4927.

of Pt(II) complexes with DNA and proteins.[27,35–38] Complexes of Pt(II) with tridentate ligands are typically not emissive or weakly emissive at RT in solution because of Pt-to-Pt intermolecular interactions or low-lying LF states.[39,40] Recently, modified $[Pt(tpy)L]^{n+}$ analogs have been designed to display enhanced emission through the substitution of the tpy ligand[41–45] or replacement with modified tridentate ligands.[46] Platinum(II) complexes have been applied to solar water splitting,[47,48] vapoluminescent sensors,[49,50] or light-emitted materials.[51]

To take advantage of the rich photophysical properties of ruthenium polyazine complexes and potential reactivity of Pt(II) complexes within a stereochemically defined tridentate coordination environment, basic studies are needed to explore the spectroscopic redox and photophysical properties of such complexes within this framework. Herein, we report the preparation, X-ray crystallographic analysis, and study of the redox, spectroscopic, and photophysical properties of the stereochemically defined mixed-metal bimetallic and trimetallic complexes $[(tpy)Ru(tppz)PtCl](PF_6)_3$ and $[ClPt(tppz)Ru(tppz)PtCl](PF_6)_4$.

Experimental Section

Materials. $RuCl_3 \cdot xH_2O$ (Alfar Aesar), K_2PtCl_4 (Alfar Aesar), 2,2′:6′,2″-terpyridine (tpy) (Aldrich), 2,3,5,6-tetrakis(2-pyridyl)pyrazine (tppz) (Aldrich), (NH_4PF_6) (Alfar Aesar), tetrabutylammonium hexafluorophosphate (Bu_4NPF_6) (Fluka), spectral, and ACS grade acetonitrile, and toluene were all used without further purification. The complexes $[(tppz)_2Ru](PF_6)_2$,[19] $[(tpy)Ru(tppz)](PF_6)_2$,[20] and $[PtCl_2(DMSO)_2]$[52] were prepared according to literature methods.

Synthesis of [(tpy)Ru(tppz)PtCl](PF$_6$)$_3$. The complex $[(tpy)Ru(tppz)PtCl](PF_6)_3$ was prepared by dropwise addition of $[(tpy)Ru(tppz)](PF_6)_2$ (51 mg, 0.050 mmol) in CH_3CN (∼10 mL) to a refluxing solution of $[Pt(DMSO)_2Cl_2]$ (84 mg, 0.40 mmol) in CH_3CN (∼10 mL) under an Ar atmosphere. The reaction mixture was heated at reflux for ∼4 h, cooled to RT, vacuum filtered, and added dropwise to an aqueous solution of 4.0 M NH_4PF_6 (∼50 mL). The violet product which precipitates upon addition to aqueous NH_4PF_6 was collected by vacuum filtration and washed with EtOH (∼20 mL), distilled H_2O (∼10 mL at 0 °C), and diethyl ether (50 mL). The product yield is 76%. ^{1}H NMR (500 MHz in CD_3CN): δ (ppm) 9.45 (J = 5.5, 1.5 Hz, 2H), 8.87 (J = 8.5 Hz, 2H), 8.86 (J = 8.5, 1.0 Hz, 2H), 8.74 (J = 8.0, 1.0 Hz, 2H), 8.63 (J = 7.8 Hz, 1H), 8.56 (J = 7.5 Hz, 2H), 8.43 (J = 8.0, 6.3, 1.7 Hz, 2H), 8.11 (J = 7.8, 5.0, 1.3 Hz, 2H), 8.01 (J = 8.5, 7.0, 1.3 Hz, 2H), 7.99 (J = 7.8, 6.3, 1.5 Hz, 2H), 7.66 (J = 6.3, 1.0 Hz, 2H), 7.48 (J = 6.2, 1.0 Hz, 2H), 7.44 (J = 7.8, 6.8, 1.5 Hz, 2H), 7.17 (J = 7.8, 6.3, 1.5 Hz, 2H). FAB-MS [m/z]calcd. $(M - PF_6)^+$: 1243.

Synthesis of [ClPt(tppz)Ru(tppz)PtCl](PF$_6$)$_4$. Using an approach similar to that for the synthesis of $[(tpy)Ru(tppz)PtCl](PF_6)_3$, the complex $[ClPt(tppz)Ru(tppz)PtCl](PF_6)_4$ was prepared by dropwise addition of $[Ru(tppz)_2](PF_6)_2$ (72 mg, 0.062 mmol) in CH_3CN (∼10 mL) to a refluxing solution of $[Pt(DMSO)_2Cl_2]$ (210 mg, 0.50 mmol) in CH_3CN (∼10 mL). The reaction mixture was heated at reflux for 4 h under an Ar atmosphere, cooled to RT, filtered, and added dropwise to an aqueous solution of 4.0 M NH_4PF_6 (∼50 mL). The violet product which forms upon addition to aqueous NH_4PF_6 is collected by vacuum filtration and washed with EtOH (∼20 mL), distilled H_2O (∼10 mL at 0 °C), and diethyl ether (50 mL). The product yield is 82%. ^{1}H NMR (500 MHz in CD_3CN): δ (ppm) 9.50 (J = 5.5 Hz, 4H), 8.90 (J = 8.5 Hz, 4H), 8.77 (J = 8.0 Hz, 4H), 8.48 (J = 7.8 Hz, 4H), 8.18 (J = 6.5 Hz, 4H), 8.06 (J = 8.5 Hz, 4H), 7.85 (br, 4H), 7.50 (br, 4H). FAB-MS [m/z]calcd. $(M - PF_6^+)$: 1772.

Methods. FAB-Mass Spectrometry. FAB mass spectral analysis was performed by M-Scan Incorporated, West Chester, PA, on a VG Analytical ZAB 2-SE high-field mass spectrometer using *m*-nitrobenzyl alcohol as a matrix.

Nuclear Magnetic Resonance (NMR) Spectroscopy. All standard ^{1}H NMR spectra were record on JEOL 500 MHz NMR spectrometer at 303 K. All the 2D spectroscopy were performed on a Varian INOVA 400 MHz NMR spectrometer at 303 K. The samples (∼5 mg) were dissolved in the CD_3CN and filtered prior to placing in NMR tubes for data collection. Chemical shifts are referenced to TMS in CD_3CN.

Electronic Absorption Spectroscopy. Spectra were generated at room temperature in a 1 cm quartz cuvette using a Hewlett-Packard 8452 diode array spectrometer with a 2 nm resolution and a spectral range of 190−820 nm. Extinction coefficients were collected in triplicate from separate solutions prepared gravimetrically and averaged.

Emission Spectroscopy. Emission spectra were recorded at RT in deoxygenated acetonitrile solutions using a modified QuantaMaster Model QM-200-45E fluorimeter from Photon Technology Inc. The system was modified to use a 150 W water-cooled xenon lamp excitation source collected at a right angle by a thermoelectrically cooled Hamamatsu 1527 photomultiplier tube operating in photon-counting mode with 0.25 nm resolution. The emission spectra were corrected for PMT response and the quantum efficiency, Φ^{em}, determined versus $[Os(bpy)_3](PF_6)_2$ (Φ^{em} = 0.00462)[53] in absorbance matched deoxygenated solutions.

Emission Lifetime Measurements. Laser-induced emission lifetime measurements were obtained on a system that uses a Photon Technology Inc. PL-2300 nitrogen laser equipped with a PL-201

(35) Wang, H. J. A.; Nathans, J.; Van Del Marel, G.; Van Boom, J. H.; Rich, A. *Nature* **1978**, *276*, 471–474.
(36) Howegrant, M.; Lippard, S. J. *Biochemistry* **1979**, *18*, 5762–5769.
(37) Peyratout, C. S.; Aldridge, T. K.; Crites, D. K.; McMillin, D. R. *Inorg. Chem.* **1995**, *34*, 4484–4489.
(38) Lippard, S. J. *Acc. Chem. Res.* **1978**, *11*, 211–217.
(39) Aldridge, T. K.; Stacy, E. M.; McMillin, D. R. *Inorg. Chem.* **1994**, *33*, 722–727.
(40) Tears, D. K. C.; McMillin, D. R. *Coord. Chem. Rev.* **2001**, *211*, 195–205.
(41) Yam, V. W. W.; Chan, K. H. Y.; Wong, K. M. C.; Zhu, N. Y. *Chem.—Eur. J.* **2005**, *11*, 4535–4543.
(42) Wilson, M. H.; Ledwaba, L. P.; Field, J. S.; McMillin, D. R. *Dalton. Trans.* **2005**, 2754–2759.
(43) McMillin, D. R.; Moore, J. J. *Coord. Chem. Rev.* **2002**, *229*, 113–121.
(44) Lai, S. W.; Lam, H. W.; Lu, W.; Cheung, K. K.; Che, C. M. *Organometallics* **2002**, *21*, 226–234.
(45) Yam, V. W. W.; Chan, K. H. Y.; Wong, K. M. C.; Chu, B. W. K. *Angew. Chem., Int. Ed.* **2006**, *45*, 6169–6173.
(46) Hu, Y. Z.; Wilson, M. H.; Zong, R. F.; Bonnefous, C.; McMillin, D. R.; Thummel, R. P. *Dalton Trans.* **2005**, 354–358.
(47) Zhang, D.; Wu, L. Z.; Zhou, L.; Han, X.; Yang, Q. Z.; Zhang, L. P.; Tung, C. H. *J. Am. Chem. Soc.* **2004**, *126*, 3440–3441.
(48) Du, P.; Schneider, J.; Jarosz, P.; Eisenberg, R. *J. Am. Chem. Soc.* **2006**, *128*, 7726.
(49) Kui, S. C. F.; Chui, S. S. Y.; Che, C. M.; Zhu, N. *J. Am. Chem. Soc.* **2006**, *128*, 8279.
(50) Wadas, T. J.; Wang, Q. M.; Kim, Y. J.; Flaschenreim, C.; Blanton, T. N.; Eisenberg, R. *J. Am. Chem. Soc.* **2004**, *126*, 16841–16849.
(51) Kui, S. C. F.; Sham, I. H. T.; Cheung, C. C. C.; Ma, C.-W.; Yan, B.; Zhu, N.; Che, C.-M.; Fu, W.-F. *Chem.—Eur. J.* **2007**, *13*, 417–435.
(52) Rice, J. H.; Williamson, A. N.; Schramm, R. F.; Wayland, B. B. *Inorg. Chem.* **1972**, *11*, 1280–4.
(53) Caspar, J. V.; Kober, E. M.; Sullivan, B. P.; Meyer, T. J. *J. Am. Chem. Soc.* **1982**, *104*, 630.

continuously tunable dye laser (360−900 nm) excitation source. The emission was passed through a monochromator and detected at a right angle to the excitation by a Hamamatsu R928 photomultiplier tube operating in direct analog mode. The signal was recorded on a LeCroy 9361 oscilloscope and the data transferred to a computer for analysis. The solutions were prepared in deoxygenated solutions. The raw data, which is an average of 200 traces, was fit to a single exponential function of the form $Y = A + B(\exp(-X/c))$, where $c = \tau = 1/k$ (s), after the initial segment of the data containing the laser pulse was discarded.

X-Ray Diffraction of [(tpy)Ru(tppz)PtCl](PF$_6$)$_3$ and [ClPt(tppz)Ru(tppz)PtCl](PF$_6$)$_4$. Black parallelepipeds of [(tpy)Ru(tppz)PtCl][PF$_6$]$_3$ were crystallized from toluene/CH_3NO_2. The chosen crystal ($0.09 \times 0.15 \times 0.25$ mm^3) was centered on the goniometer of an Oxford Diffraction Gemini diffractometer equipped with a Sapphire 3 CCD detector and operating with Mo Kα radiation. The data collection routine, unit cell refinement, and data processing were carried out with the program CrysAlisPro.[54] The Laue symmetry and systematic absences were consistent with the monoclinic space group *Cc* and *C*2/*c*. The centric space group *C*2/*c* was chosen. The structure was solved by direct methods and refined using SHELXTL NT.[55] The asymmetric unit of the structure comprises one crystallographically independent [(tpy)Ru(tppz)PtCl][PF$_6$]$_3$ salt. After the [(tpy)Ru(tppz)PtCl][PF$_6$]$_3$ was located, the residual electron density in remaining void spaces suggested the presence of disordered solvent. Various attempts were made to model or correct for this disorder, including multiposition solvent disorder and running the PLATON routine SQUEEZE[56] to subtract out the solvent electron density. With most models used, the goodness-of-fit suggested we were overfitting the data, yet the refinement model did not improve substantially. In the final refinement, the solvent was modeled as a toluene disordered over two positions with relative occupancies of 74(2)% and 26(2)%. The phenyl ring of the toluene molecule was restrained to fit a hexagon. The toluene atoms were refined isotropically; all remaining non-hydrogen atoms were refined anisotropically and a riding model was used for all hydrogen atoms.

Black plates of [ClPt(tppz)Ru(tppz)PtCl][PF$_6$]$_4$ were crystallized from CH_3CN/Et_2O. The chosen crystal ($0.01 \times 0.11 \times 0.29$ mm^3) was centered on the goniometer of an Oxford Diffraction Gemini diffractometer equipped with a Sapphire 3 CCD detector and operating with Mo Kα radiation. The data collection routine, unit cell refinement, and data processing were carried out with the program CrysAlisPro.[54] The Laue symmetry and systematic absences were consistent with the monoclinic space group $P2_1/c$. The structure was solved by direct methods and refined using SHELXTL NT.[55] The asymmetric unit of the structure comprises one crystallographically independent [ClPt(tppz)Ru(tppz)PtCl][PF$_6$]$_4$ salt. After the [ClPt(tppz)Ru(tppz)PtCl][PF$_6$]$_4$ was located, residual electron density in remaining void spaces suggested the presence of disordered solvent. Various attempts were made to model or correct for this disorder, including a variety of multiposition disorder models for the ether molecule and PF_6 anions, as well as running the PLATON routine SQUEEZE[56] to subtract out the ether electron density. Regardless of the model used, the *R*-values tended to improve, but the anisotropic displacement parameters remained unsatisfactory. Presumably the small crystal size and potential dynamic motion in the solvents and PF_6^- limit the data quality. In the final refinement, the solvent was modeled as two CH_3CN molecules and one Et_2O molecule without disorder. The Et_2O atoms were refined isotropically; all remaining non-hydrogen atoms were refined anisotropically, and a riding model was used for all hydrogen atoms.

(54) *CrysAlis*, version 1.171; Oxford Diffraction: Wroclaw, Poland, 2007.
(55) Sheldrick, G. M. *SHELXTL NT*, version 6.12; Bruker Analytical X-ray Systems, Inc.: Madison, WI, 2001.
(56) Spek, A. L. *J. Appl. Crystallogr.* **2003**, *36*, 7–13.

Results and Discussion

Synthesis. The supramolecular complexes, [(tpy)Ru(tppz)PtCl](PF$_6$)$_3$ and [ClPt(tppz)Ru(tppz)PtCl](PF$_6$)$_4$, have been prepared in good yield using a building block approach with coordination of the Pt center being the final step. The complexes have been characterized by FAB mass spectrometry, X-ray crystallography, and ^{1}H NMR spectroscopy. The supramolecular assemblies provide a TL−LA−BL−RM (TL = terminal ligand) architecture in the bimetallic complex, [(tpy)Ru(tppz)PtCl](PF$_6$)$_3$, and a RM−BL−LA−BL−RM architecture in the trimetallic complex, [ClPt(tppz)Ru(tppz)PtCl](PF$_6$)$_4$. The bimetallic and trimetallic complexes are unique in their coupling of Ru LA units to a Pt(II) center in a stereochemically defined coordination environment. The tppz BL provides a low-lying π^*-acceptor orbital affording a stabilized ^{3}MLCT state and an emissive trimetallic complex. The characterization by ^{1}H NMR spectroscopy is atypical for Ru,Pt polyazine bridged complexes made possible by the tridentate, structurally determined molecular architecture. The X-ray crystallographic analysis of these complexes is also unusual as typical polyazine-bridged complexes exist as mixtures of many isomers. The [(tpy)Ru(tppz)PtCl](PF$_6$)$_3$ and [ClPt(tppz)Ru(tppz)PtCl](PF$_6$)$_4$ systems display mass spectra consistent with their formulation. Typically complexes of this type display FAB mass spectral characteristics of the metal complex with loss of anions and often intact ligands. The FAB mass spectral analysis shows peaks for the $[M - PF_6]^+$ *m*/*z* of 1243 for bimetallic and 1772 for the trimetallic. The details of the mass spectra are provided in the Supporting Information.

Crystal Structure Determination. The solid state structures of [(tpy)Ru(tppz)PtCl](PF$_6$)$_3$ and [ClPt(tppz)Ru(tppz)PtCl][PF$_6$]$_4$ were determined to establish the geometry about the metal centers and the bonding modes of the tppz ligands. The experimental crystallographic data and selected bond lengths and angles for [(tpy)Ru(tppz)PtCl](PF$_6$)$_3$ and [ClPt(tppz)Ru(tppz)PtCl][PF$_6$]$_4$ are given in Tables 1–3, and the perspective views are illustrated in Figure 1. The metal coordination complexes have overall positive charges, and there are hexafluorophosphate ions that serve to balance these charges. The presence of disordered solvent, anions, or both and the small size of the crystals limit the quality of the fit of our data. Both complexes display distorted octahedral geometry on the Ru center and distorted square planar geometry on the Pt center, with the proposed tridentate bridging coordination of the tppz. The typical distortion of the tppz ligand to remove steric interactions of the hydrogens in the 3-positions (H^3) on the pyridine rings is observed. Interestingly, the two complexes show different intermolecular interactions. The complex [(tpy)Ru(tppz)PtCl](PF$_6$)$_3$ shows intermolecular interactions between the two Pt centers of the two independent molecules in the unit cell with a Pt···Pt distance of 3.3218(5) Å. Analysis

Table 1. Crystallographic Data Collection and Structure Refinement Parameters for $[(tpy)Ru(tppz)PtCl](PF_6)_3$ and $[ClPt(tppz)Ru(tppz)PtCl](PF_6)_4$

identification code	$[(tpy)Ru(tppz)PtCl](PF_6)_3$	$[ClPt(tppz)Ru(tppz)PtCl][PF_6]\cdot 2CH_3CN\cdot Et_2O$
empirical formula	$[C_{39}H_{27}ClN_9PtRu][PF_6]_3\cdot C_7H_8$	$C_{56}H_{48}Cl_2F_{24}\ N_{14}OP_4Pt_2Ru$
fw	1480.35	2075.11
space group	*C*2/*c*	$P2_1/c$
a (Å)	16.4811(3)	12.4793(2)
b (Å)	31.2657(7)	24.3668(5)
c (Å)	19.9039(3)	22.5775(4)
α (deg)	90	90
β (deg)	94.364(2)	103.4360(10)
γ (deg)	90	90
vol (Å^3)	10 226.6(3)	6 677.5(2)
Z	8	4
temp (K)	100(2)	100(2)
density (calcd, Mg/m^3)	1.923	2.064
wavelength (Å)	0.71073	0.71073
abs coeff (mm^{-1})	3.286	4.700
final R indices	R1 = 0.0432, wR2 = 0.1282	R1 = 0.0605, wR2 = 0.1111
R indices (all data)	R1 = 0.0596, wR2 = 0.1384	R1 = 0.0955, wR2 = 0.1268

Table 2. Selected Bond Lengths (Å) and Angles (deg) for $[(tpy)Ru(tppz)PtCl](PF_6)_3$

Pt(1)−N(7)	2.012(6)	N(2)−Ru(2)−N(1)	78.5(2)
Pt(1)−N(8)	1.947(6)	N(5)−Ru(2)−N(6)	80.3(2)
Pt(1)−N(9)	1.999(6)	N(8)−Pt(1)−N(9)	81.5(2)
Pt(1)−Cl(1)	2.2971(19)	N(8)−Pt(1)−Cl(1)	179.58(17)
Ru(2)−N(1)	2.066(6)	C(19)−C(20)−C(21)−C(22)	18.1(11)
Ru(2)−N(2)	1.989(6)	C(20)−C(21)−C(22)−C(23)	21.2(12)
Ru(2)−N(3)	2.084(6)	C(21)−C(22)−C(23)−C(24)	17.0(11)
Ru(2)−N(4)	2.066(5)	C(31)−C(32)−C(33)−C(34)	19.7(11)
Ru(2)−N(5)	1.951(6)	C(32)−C(33)−C(34)−C(35)	20.7(12)
Ru(2)−N(6)	2.050(5)	C(33)−C(34)−C(35)−C(36)	14.4(11)

Table 3. Selected Bond Lengths (Å) and Angles (deg) for $[ClPt(tppz)Ru(tppz)PtCl](PF_6)_4$

Pt(1)−N(1)	1.923(8)	N(1)−Pt(1)−Cl(1)	177.4(2)
Pt(1)−N(3)	1.982(8)	N(1)−Pt(1)−N(3)	82.0(3)
Pt(1)−N(4)	1.999(9)	N(5)−Ru(1)−N(6)	157.2(3)
Pt(1)−Cl(1)	2.291(2)	N(8)−Pt(2)−N(12)	81.4(3)
Pt(2)−N(8)	1.928(7)	N(8)−Pt(2)−Cl(2)	179.7(3)
Pt(2)−N(12)	1.987(9)	N(9)−Ru(1)−N(10)	158.0(3)
Pt(2)−N(11)	2.006(10)	C(2)−C(1)−C(9)−C(8)	22.4(17)
Pt(2)−Cl(2)	2.294(2)	C(9)−C(1)−C(2)−C(15)	27.1(17)
Ru(1)−N(2)	1.982(8)	C(1)−C(2)−C(15)−C(16)	11.8(16)
Ru(1)−N(5)	2.072(8)	C(2)−C(15)−C(16)−C(17)	173.9(10)
Ru(1)−N(6)	2.086(8)	C(3)−C(4)−C(20)−C(21)	19.8(16)
Ru(1)−N(7)	1.986(8)	C(4)−C(3)−C(14)−C(13)	7.2(16)
Ru(1)−N(9)	2.070(8)	C(14)−C(3)−C(4)−C(20)	30.6(17)
Ru(1)−N(10)	2.083(7)	C(25)−C(26)−C(39)−C(40)	14.7(18)
N(2)−Ru(1)−N(7)	178.9(3)	C(26)−C(25)−C(33)−C(32)	11.5(17)
N(2)−Ru(1)−N(5)	78.9(3)	C(28)−C(44)−C(45)−C(46)	173.7(9)
N(7)−Ru(1)−N(9)	78.7(3)	C(28)−C(27)−C(38)−C(37)	16.2(16)
		C(33)−C(25)−C(26)−C(39)	23.9(17)

of the crystal packing of $[ClPt(tppz)Ru(tppz)PtCl](PF_6)_4$ reveals that the molecules are arranged without this close Pt-to-Pt intermolecular interaction.

^{1}H NMR Spectroscopy. The ^{1}H NMR spectra for $[(tpy)Ru(tppz)PtCl](PF_6)_3$ and $[ClPt(tppz)Ru(tppz)PtCl](PF_6)_4$ were recorded in CD_3CN at room temperature, Figure 2. The stereochemically defined nature of these complexes make the complete assignment possible. The assignments were confirmed on the basis of the coupling constants, ^{1}H−^{1}H correlation spectroscopy (^{1}H−^{1}H COSY), nuclear overhauser effect spectroscopy (NOESY), and comparison to the known systems, $[(tpy)Ru(tppz)](PF_6)_2$, $[Ru(tpy)_2](PF_6)_2$, $[Ru(tppz)_2](PF_6)_2$, tpy, and tppz. The chemical shifts of $[(tpy)Ru(tppz)](PF_6)_2$, $[Ru(tppz)_2](PF_6)_2$, $[(tpy)Ru(tppz)PtCl](PF_6)_3$, $[ClPt(tppz)Ru(tppz)PtCl](PF_6)_4$, $[Ru(tpy)_2]^{2+}$, tpy, and tppz and their coupling constants are summarized in the Supporting Information. The numbering scheme used for the assignments of the protons is given in Figure 3. The chemical shifts of the protons in these systems are impacted by the electron-withdrawing effects imposed by the ligand and coordinated metal and ring−current effects.[57,58]

The ^{1}H NMR spectrum of $[(tpy)Ru(tppz)PtCl](PF_6)_3$ in CD_3CN at room temperature agrees well with the solid state structure and displays 14 nonequivalent proton resonances. The H^4A proton is distinct and appears as a virtual triplet at δ 8.63 with half the integral intensity of the other protons. Upon assignment of H^4A, the doublet at δ 8.87 can be easily assigned to H^3A using ^{1}H−^{1}H COSY. The distinction between protons of rings B and C was achieved using NOESY, while the assignments of the sets of protons on each individual ring were achieved using ^{1}H−^{1}H COSY. For example, the NOESY spectrum of $[(tpy)Ru(tppz)PtCl](PF_6)_3$ indicated through space interactions between H^3A and the doublet at δ 8.56 attributed to H^3B. The rest of the protons of ring B were identified based on this interaction and ^{1}H−^{1}H COSY correlations. The resonances at δ 7.99, 7.44, and 7.66 display the expected splitting pattern for H^4B, H^5B, and H^6B, respectively. The individual assignments of the $(tpy)Ru^{II}$ component of $[(tpy)Ru(tppz)PtCl](PF_6)_3$, are comparable with those of the $(tpy)Ru^{II}$ component of $[(tpy)Ru(tppz)](PF_6)_2$ and $[Ru(tpy)_2]^{2+}$,[57] Supporting Information. The H^6 protons of rings C and D in $[(tpy)Ru(tppz)](PF_6)_2$, appear as doublet of doublets, with H^6C shifted downfield (δ 8.73) relative to H^6D (δ 7.40), consistent with the electron-withdrawing effect imposed by Ru on ring C. The significant downfield shift of H^6C (δ 8.73) relative to H^6B (δ 7.59) in $[(tpy)Ru(tppz)](PF_6)_2$, maybe a combination effect of the coordination of ring C to Ru and its attachment to the pyrazine ring of tppz, shifting the H^6C resonance to low field. Coordination of a Pt center to ring D in $[(tpy)Ru(tppz)PtCl](PF_6)_3$, leads to a significant downfield shift in H^6D (δ 9.45). Using ^{1}H−^{1}H COSY, the resonances at δ 8.74, 8.43, and 8.11 were assigned to H^3D, H^4D, and H^5D, respectively, of $[(tpy)Ru(tppz)PtCl](PF_6)_3$. Consistent with Pt coordination, H^3D, H^4D, and H^5D of $[(tpy)Ru(tppz)PtCl](PF_6)_3$ occur significantly downfield relative to the corresponding protons of $[(tpy)Ru(tppz)](PF_6)_2$. By contrast, the upfield shift of H^6C in $[(tpy)Ru(tppz)PtCl](PF_6)_3$, ($\delta$ 7.48) relative to $[(tpy)Ru(tppz)](PF_6)_2$ (δ 8.73) is caused by pronounced shielding of H^6C when ring D is complexed to Pt in $[(tpy)Ru(tppz)PtCl](PF_6)_3$ relative to the free tppz of $[(tpy)Ru(tppz)](PF_6)_2$. This shielding is imposed by ring current effects as H^6C lies directly above the π-cloud of ring A in $[(tpy)Ru(tppz)PtCl](PF_6)_3$. The remaining resonances at δ 8.86, 8.01, and 7.17 were assigned to H^3C, H^4C, and H^5C of $[(tpy)Ru(tppz)PtCl](PF_6)_3$ using ^{1}H−^{1}H COSY,

(57) Thummel, R. P.; Jahng, Y. *Inorg. Chem.* **1986**, *25*, 2527–2534.
(58) Laine, P.; Bedioui, F.; Ochsenbein, P.; Marvaud, V.; Bonin, M.; Amouyal, E. *J. Am. Chem. Soc.* **2002**, *124*, 1364–1377.

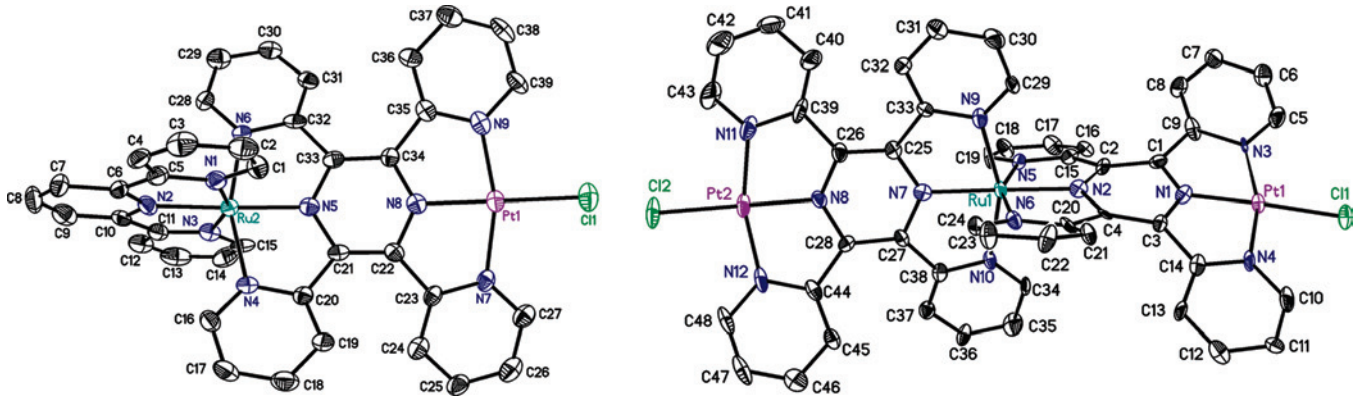

Figure 1. Fifty percent thermal ellipsoid representations of the cations $[(tpy)Ru(tppz)PtCl]^{3+}$ (left) and $[ClPt(tppz)Ru(tppz)PtCl]^{4+}$ (right) (tpy = 2,2′:6′,2″-terpyridine, tppz = 2,3,5,6-tetrakis(2-pyridyl)pyrazine).

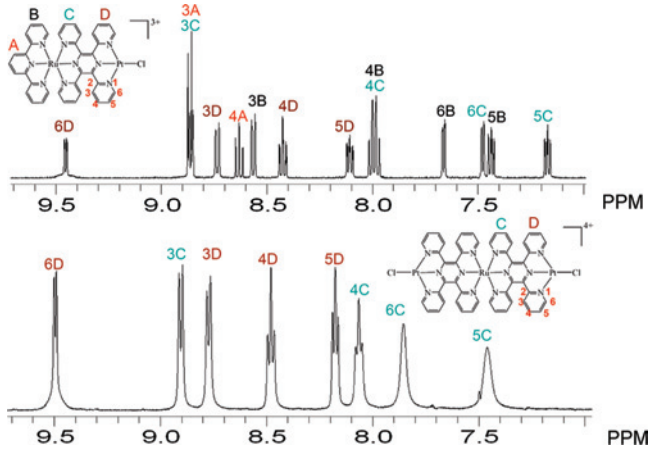

Figure 2. ^{1}H NMR spectra of mixed−metal supramolecular complexes $[(tpy)Ru(tppz)PtCl](PF_6)_3$ (top) and $[ClPt(tppz)Ru(tppz)PtCl](PF_6)_4$ (bottom) recorded in CD_3CN at RT (tpy = 2,2′:6′,2″-terpyridine and tppz = 2,3,5,6-tetrakis(2-pyridyl)pyrazine).

Supporting Information. The NOESY spectrum of $[(tpy)Ru(tppz)PtCl](PF_6)_3$ revealed through space interactions between H^3C and H^3D, consistent with our assignments.

The ^{1}H NMR spectrum of $[ClPt(tppz)Ru(tppz)PtCl](PF_6)_4$ revealed eight resonances consistent with its structure. The NMR spectrum of $[ClPt(tppz)Ru(tppz)PtCl](PF_6)_4$ is simplified relative to $[(tpy)Ru(tppz)PtCl](PF_6)_3$ because of the presence of only tppz protons. At room temperature in CD_3CN, the ^{1}H NMR spectrum of $[ClPt(tppz)Ru(tppz)PtCl](PF_6)_4$, reveals resonances resulting from protons of rings C and D that are quite comparable to $[(tpy)Ru(tppz)PtCl](PF_6)_3$, Supporting Information. A unique feature in the ^{1}H NMR spectrum of $[ClPt(tppz)Ru(tppz)PtCl](PF_6)_4$ is the broadening of the resonances at δ 7.85 and 7.50 of protons H^6C and H^5C, respectively. Variable-temperature ^{1}H NMR spectroscopy in CD_3CN at −20 °C reveal two individual resonances for H^6C and H^5C, reflective of slow exchange at −20 °C, Figure 4. By contrast, the ^{1}H NMR spectrum of $[ClPt(tppz)Ru(tppz)PtCl](PF_6)_4$ at 60 °C show sharp resonances with the expected splitting pattern for H^6C and H^5C consistent with rapid exchange at this temperature, Figure 4. As illustrated by X-ray crystallography, the H^3D to H^3C steric repulsion prevents the tppz ligands from being planar and the ligand distorts to remove this interaction. Each of the two tppz ligands in this complex twists to remove the H^3C to H^3D steric repulsions. These distortions may significantly impact the ring current effect experienced by H^6C and H^5C. The relative distortions of each tppz ligand can provide inequivalent positions for the H^6C and H^5C protons, and their interconversion at RT may account for the observed broadening of these resonances. Alternatively, the presence of intermolecular interactions in solution is expected in $Pt^{II}(NNN)Cl$ subunits. Similar interactions in $[ClPt(tppz)Ru(tppz)PtCl](PF_6)_4$ can lead to inequivalent H^6C and H^5C environments that can rapidly exchange at RT.

Electrochemistry. Mixed-metal complexes of polyazine ligands display rich electrochemistry with reversible metal-based oxidations for the $Ru^{II/III}$ processes and ligand-based reductions, with BL reductions occurring at more-positive potential. The electrochemical properties of the title $[(tpy)Ru(tppz)PtCl](PF_6)_3$ and $[ClPt(tppz)Ru(tppz)PtCl](PF_6)_4$, along with related tppz complexes, are given in Table 4.

The electrochemistry of $[(tpy)Ru(tppz)PtCl](PF_6)_3$ and $[ClPt(tppz)Ru(tppz)PtCl](PF_6)_4$ consist of reversible $Ru^{II/III}$-based oxidations and ligand based reductions, Table 4. The Ru center coordinated to two tppz ligands in $[ClPt(tppz)Ru(tppz)PtCl](PF_6)_4$ is more difficult to oxidize (1.83 V vs Ag/AgCl) relative to $[(tpy)Ru(tppz)PtCl](PF_6)_3$ (1.63 V vs Ag/AgCl), consistent with the better π-accepting ability of the tppz ligand relative to tpy. For comparison, the $Ru^{II/III}$ couple of the monometallic synthon, $[Ru(tppz)_2](PF_6)_2$, is also shifted to more positive potential by 120 mV relative to $[(tpy)Ru(tppz)](PF_6)_2$. Platinum coordination to the monometallic synthons $[(tpy)Ru(tppz)](PF_6)_2$ and $[Ru(tppz)_2](PF_6)_2$ also impacts the $Ru^{II/III}$ oxidation as evidenced by the $Ru^{II/III}$ couple of $[ClPt(tppz)Ru(tppz)PtCl](PF_6)_4$ occurring at the most positive potential. The reductive electrochemistry of $[(tpy)Ru(tppz)PtCl](PF_6)_3$ and $[ClPt(tppz)Ru(tppz)PtCl](PF_6)_4$ display tppz-based reductions that occur at significantly more positive potentials compared to their monometallic synthons, $[(tpy)Ru(tppz)](PF_6)_2$ and $[Ru(tppz)_2](PF_6)_2$, respectively, Table 4. This positive shift implies that the coordination of Pt(II) to the remote site of tppz affords significant stabilization of the tppz(π^*) acceptor orbitals in $(tpy)Ru(tppz)PtCl](PF_6)_3$ and $[ClPt(tppz)Ru(tppz)PtCl](PF_6)_4$. For example, the $tppz^{0/-}$

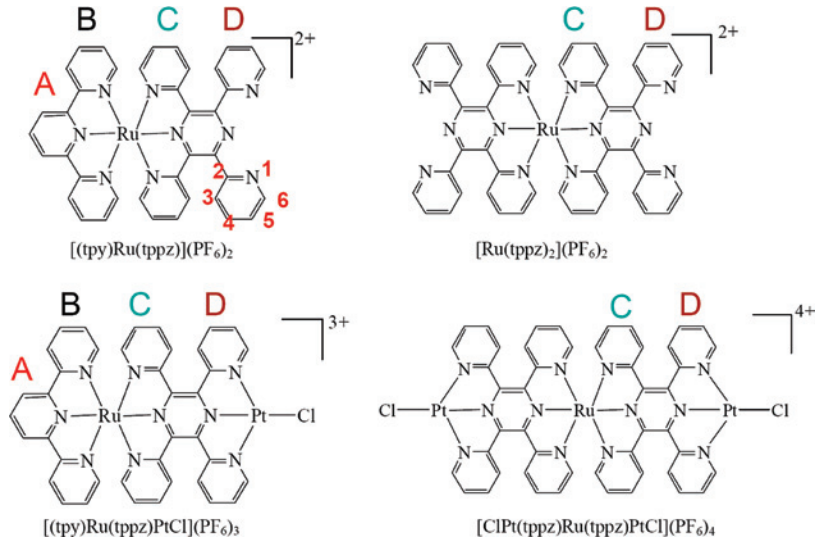

Figure 3. Numbering scheme used for labeling protons in $[(tpy)Ru(tppz)](PF_6)_2$, $[Ru(tppz)_2](PF_6)_2$, $[(tpy)Ru(tppz)PtCl](PF_6)_3$, and $[ClPt(tppz)Ru(tppz)PtCl](PF_6)_4$ (tpy = 2,2″-terpyridine, tppz = 2,3,5,6-tetrakis(2-pyridyl)pyrazine).

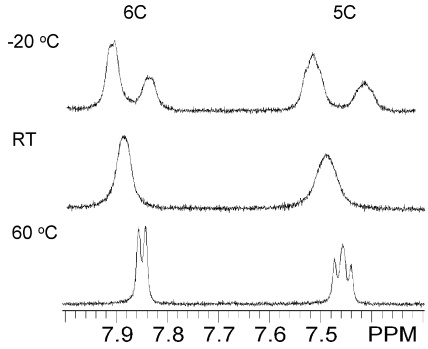

Figure 4. Selected region of the 400 MHz ^{1}H NMR spectrum of $[ClPt(tppz)Ru(tppz)PtCl](PF_6)_4$ at −20, RT and 60 °C showing slow, intermediate, and rapid exchange regimes.

Table 4. Electrochemical Data for Ru(II) and Ru(II),Pt(II) Complexes of the Tridentate Bridging Ligand tppz (tppz = 2,3,5,6-tetrakis(2-pyridyl)pyrazine)[a]

compound	$E_{1/2}$ (V vs Ag/AgCl)	assignment
$[Ru(tppz)_2](PF_6)_2$[b]	1.54	$Ru^{II/III}$
	−0.85	$tppz^{0/-}$
	−1.06	$tppz^{0/-}$
$[(tpy)Ru(tppz)](PF_6)_2$[c]	1.42	$Ru^{II/III}$
	−0.95	$tppz^{0/-}$
	−1.39	$tpy^{0/-}$
$[(tpy)Ru(tppz)Ru(tppz)](PF_6)_4$[c]	1.51	$Ru^{II/III}$
	−0.30	$tppz^{0/-}$
$[(tpy)Ru(tppz)PtCl](PF_6)_3$	1.63	$Ru^{II/III}$
	−0.16	$tppz^{0/-}$
	−0.70	$tppz^{-/2-}$
$[ClPt(tppz)Ru(tppz)PtCl](PF_6)_4$	1.83	$Ru^{II/III}$
	−0.03	$tppz^{0/-}$
	−0.17	$tppz^{0/-}$

[a] Recorded in 0.1 M Bu_4NPF_6 CH_3CN with E in V vs Ag/AgCl (0.29 V vs NHE), tpy = 2,2′:6′,2″-terpyridine and tppz =2,3,5,6-tetrakis(2-pyridyl)-pyrazine. [b] Ref 19 [c] Ref 20.

couple shifts from −0.95 and −0.85 V vs Ag/AgCl in $[(tpy)Ru(tppz)](PF_6)_2$ and $[Ru(tppz)_2](PF_6)_2$, respectively, to −0.16 and −0.03 in $[(tpy)Ru(tppz)PtCl](PF_6)_3$ and $[ClPt(tppz)Ru(tppz)PtCl](PF_6)_4$, respectively. Stabilization of the tppz(π^*) orbital upon Pt coordination is significantly larger than with Ru coordination where the $tppz^{0/-}$ process occurs at −0.30 V vs Ag/AgCl for $[(tpy)Ru(tppz)Ru(tppz)](PF_6)_4$.[20] The electrochemical properties of $[(tpy)Ru(tppz)PtCl](PF_6)_3$ and $[ClPt(tppz)Ru(tppz)PtCl](PF_6)_4$ establish a Ru(dπ) HOMO (highest-occupied molecular orbital) and tppz (π^*) LUMO (lowest-unoccupied molecular orbital) in these structural motifs. The electrochemistry predicts a lowest-lying Ru(dπ) → tppz(π^*) ^{3}MLCT excited state with a lower-energy MLCT for $[(tpy)Ru(tppz)PtCl](PF_6)_3$.

Electronic Absorption and Emission Spectroscopy. The complexes $[(tpy)Ru(tppz)PtCl](PF_6)_3$ and $[ClPt(tppz)Ru(tppz)PtCl](PF_6)_4$ and their monometallic synthons, $[(tpy)Ru(tppz)](PF_6)_2$ and $[Ru(tppz)_2](PF_6)_2$, are efficient light absorbers displaying intraligand (IL) $\pi \rightarrow \pi^*$ transitions in the UV and MLCT transitions in the visible, with the lowest-energy transition being Ru(dπ) → tppz(π^*) MLCT in nature, Figure 5. Consistent with the stabilization of tppz(π^*) orbital upon Pt coordination, the Ru(dπ) → tppz(π^*) MLCT transitions are red-shifted in $[(tpy)Ru(tppz)PtCl](PF_6)_3$ (λ_{max}^{abs} = 530 nm) and $[ClPt(tppz)Ru(tppz)PtCl](PF_6)_4$ (λ_{max}^{abs} = 538 nm) relative to their monometallic synthons. This stabilization of the tppz(π^*) orbital is consistent with the positive shift of the $tppz^{0/-}$ couple, as observed in the electrochemistry of $[(tpy)Ru(tppz)PtCl](PF_6)_3$ and $[ClPt(tppz)Ru(tppz)PtCl](PF_6)_4$, relative to their monometallic synthons. The spectroscopic properties of $[(tpy)Ru(tppz)PtCl](PF_6)_3$ and $[ClPt(tppz)Ru(tppz)PtCl](PF_6)_4$ suggests that upon light absorption, charge transfer is promoted toward the coordinated Pt center to the tppz BL.

Ruthenium polyazine complexes often possess lowest-lying ^{3}MLCT states that are typically emissive. The prototypical bis-tridentate complex $[Ru(tpy)_2]^{2+}$ is not emissive. This is attributed to the presence of low-lying ligand field (LF) states that are thermally accessible at room temperature leading to rapid deactivation of the Ru(dπ) → tpy(π^*) ^{3}MLCT state. Ruthenium complexes of the tridentate BL tppz have been shown to be

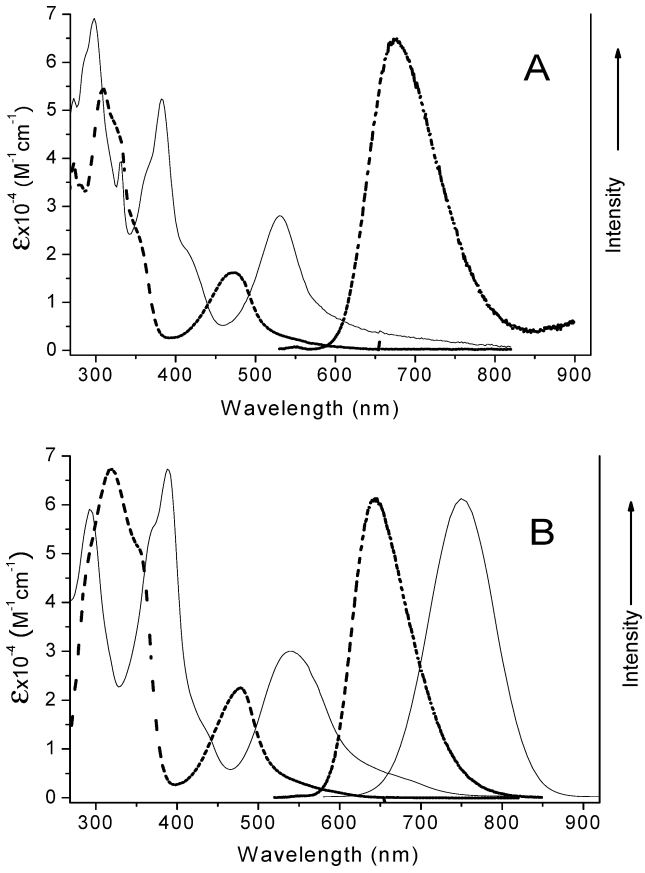

Figure 5. Electronic absorption and emission spectra for the mixed-metal supramolecular complexes and their monometallic synthons $[(tpy)Ru(tppz)](PF_6)_2$ (---) and $[(tpy)Ru(tppz)PtCl](PF_6)_3$ (—) (A) and $[Ru(tppz)_2](PF_6)_2$ (---) and $[ClPt(tppz)Ru(tppz)PtCl](PF_6)_4$ (—) (B) measured in CH_3CN at RT (tpy = 2,2′:6′,2″-terpyridine and tppz = 2,3,5,6-tetrakis(2-pyridyl)pyrazine).

emissive because of stabilization of the Ru(dπ) → tppz(π^*) ^{3}MLCT state, which limits thermal population of the ^{3}LF state. The RT emission spectra recorded in deoxygenated CH_3CN solutions of the monometallic complexes $[(tpy)Ru(tppz)](PF_6)_2$ and $[Ru(tppz)_2](PF_6)_2$ and the trimetallic complex, $[ClPt(tppz)Ru(tppz)PtCl](PF_6)_4$, are shown in Figure 5. The complexes $[(tpy)Ru(tppz)](PF_6)_2$ and $[Ru(tppz)_2](PF_6)_2$ emit at 668 and 646 nm, respectively. The trimetallic complex $[ClPt(tppz)Ru(tppz)PtCl](PF_6)_4$ displays a Ru(dπ) → tppz(π^*) ^{3}MLCT emission centered at 754 nm with an excited-state lifetime (τ) of 80 ns and Φ^{em} of 5.4×10^{-4}. The photophysical properties of $[ClPt(tppz)Ru(tppz)PtCl](PF_6)$ is comparable with $[(tpy)Ru(tppz)Ru(tppz)](PF_6)_4$: $\lambda_{max}^{em} = 830$ nm, $\tau = 100$ ns, and $\Phi^{em} = 4.0 \times 10^{-4}$.[20] The Ru(d$\pi$) → tppz($\pi^*$) ^{3}MLCT emission of $[ClPt(tppz)Ru(tppz)PtCl](PF_6)_4$ complex is significantly red-shifted relative to $[Ru(tppz)_2](PF_6)_2$, consistent with the stabilized tppz(π^*)-orbital upon Pt(II) coordination. The intense emission of $[ClPt(tppz)Ru(tppz)PtCl](PF_6)_4$ affords a probe into its excited-state reactivity and the 80 ns lifetime is a significant time for excited-state reactions. By contrast, $[(tpy)Ru(tppz)PtCl](PF_6)_3$ does not display a detectable emission under the same conditions. This difference in excited-state properties of $[(tpy)Ru(tppz)PtCl](PF_6)_3$ and $[ClPt(tppz)Ru(tppz)PtCl](PF_6)_4$ complexes is an interesting result imparted by the difference in their structures. When a CH_3CN solution of $[(tpy)Ru(tppz)PtCl](PF_6)_3$ is diluted to below 2.5×10^{-5} M, an extremely weak emission is observed at 810 nm. Platinum terpyridine complexes are known to undergo intermolecular Pt···Pt interactions that lead to quenching of the otherwise emissive ^{3}MLCT excited states. The Pt···Pt interactions in $[(tpy)Ru(tppz)PtCl](PF_6)_3$ to quench the ^{3}MLCT excited state requires the assembly of only two molecules, while $[ClPt(tppz)Ru(tppz)PtCl](PF_6)_4$ requires large aggregates to quench all the ^{3}MLCT states on the two tppz ligands. Interestingly, such Pt···Pt interactions were observed in the solid state for $[(tpy)Ru(tppz)PtCl](PF_6)_3$. Solid state emission was also probed and $[ClPt(tppz)Ru(tppz)PtCl](PF_6)_4$ maintains the characteristic ^{3}MLCT emission, while $[(tpy)Ru(tppz)PtCl](PF_6)_3$ does not display a detectable emission in the solid state.

Conclusions

The mixed-metal complexes $[(tpy)Ru(tppz)PtCl](PF_6)_3$ and $[ClPt(tppz)Ru(tppz)PtCl](PF_6)_4$ represent unique, stereochemically defined complexes of Ru^{II} and Pt^{II} that display interpretable ^{1}H NMR spectra while maintaining the efficient light-absorbing properties of typical Ru,Pt polyazine complexes. These assemblies are prepared using a building-block method. The mixed-metal complexes display very low-energy tppz(π^*)-acceptor orbitals, significantly more stabilized than typically seen for Os(II) or Ru(II) bis-chelation. The complexes are efficient light absorbers with intense transitions throughout the UV and visible with the lowest transition being MLCT in nature to the tppz acceptor orbital. In marked contrast to most tridentate complexes of Ru and the majority of Ru,Pt complexes, the tppz-bridged complex $[ClPt(tppz)Ru(tppz)PtCl](PF_6)_4$, displays an intense visible emission at $\lambda_{max}^{em} = 754$ nm with $\tau = 80$ ns at RT, characteristic of a Ru → μ-tppz ^{3}MLCT emissive state. The closely related complex $[(tpy)Ru(tppz)PtCl](PF_6)_3$ displays only an extremely weak emission in CH_3CN solution and no detectable emission in the solid state. The presence of the two Pt sites in one molecule prohibits the Pt-to-Pt interaction from simultaneously quenching both Ru → BL CT excited states, a design consideration that should be generally applicable. X-ray crystallographic analysis of these systems represents only a handful of crystallographically characterized Ru,Pt complexes. This X-ray crystallographic analysis verifies the identity of $[(tpy)Ru(tppz)PtCl](PF_6)_3$ and $[ClPt(tppz)Ru(tppz)PtCl](PF_6)_4$ with Pt···Pt interactions between the individual molecules of the unit cell in $[(tpy)Ru(tppz)PtCl](PF_6)_3$. The remote chloride ligands on the Pt site give the mixed-metal complexes an easily substituted site on this reactive metal. The coupling of a Ru light-absorbing metal to a reactive Pt metal in a stereochemically defined structural motif holds promise to expand the knowledge of the ground and excited-state properties of mixed-metal complexes with systems that are single isomers. The study of this and related Ru,Pt complexes is ongoing in our laboratory.

Acknowledgment. S.Z. thanks Dr. Ran Miao and Dr. Mark Elvington for their assistance in the collection of the

photophysical data and Prof. Brenda Winkel, Prof. Paul Deck, and Dr. Shugeng Cao for helpful discussions. Acknowledgement is made to the Chemical Sciences, Geosciences and Biosciences Division, Office of Basic Energy Sciences, Office of Science, U.S. Department of Energy for their generous support of this research.

Supporting Information Available: A synthetic scheme, mass spectrometry, and NMR spectra including $^{1}H-^{1}H$ COSY and NOESY, tables of ^{1}H NMR data, CIF files, and tables of selected bond angles. This material is available free of charge via the Internet at http://pubs.acs.org.

IC7023296